Interaction of hydrogen with actinide dioxide (111) surfaces

James T. Pegg [iD], Ashley E. Shields [iD], Mark T. Storr, David O. Scanlon [iD], and Nora H. de Leeuw [iD]

View Online   Export Citation   CrossMark

ARTICLES YOU MAY BE INTERESTED IN

A consistent and accurate ab initio parametrization of density functional dispersion correction (DFT-D) for the 94 elements H-Pu
The Journal of Chemical Physics **132**, 154104 (2010); https://doi.org/10.1063/1.3382344

Hybrid functionals based on a screened Coulomb potential
The Journal of Chemical Physics **118**, 8207 (2003); https://doi.org/10.1063/1.1564060

Investigation of near-surface defects of nanodiamonds by high-frequency EPR and DFT calculation
The Journal of Chemical Physics **150**, 134702 (2019); https://doi.org/10.1063/1.5085351

Interaction of hydrogen with actinide dioxide (111) surfaces

View Online   Export Citation   CrossMark

James T. Pegg,[1,2,a] (ID) Ashley E. Shields,[3] (ID) Mark T. Storr,[2] David O. Scanlon,[1,4,5] (ID) and Nora H. de Leeuw[1,6] (ID)

AFFILIATIONS

[1] Department of Chemistry, University College London, 20 Gordon Street, London WC1H 0AJ, United Kingdom
[2] Atomic Weapons Establishment (AWE) Plc, Aldermaston, Reading RG7 4PR, United Kingdom
[3] Oak Ridge National Laboratory, One Bethel Valley Road, Oak Ridge, Tennessee 37831, USA
[4] Diamond Light Source Ltd., Diamond House, Harwell Science and Innovation Campus, Didcot, Oxfordshire OX11 0DE, United Kingdom
[5] Thomas Young Centre, University College London, Gower Street, London WC1E 6BT, United Kingdom
[6] School of Chemistry, Cardiff University, Main Building, Park Place, Cardiff CF1D 3AT, United Kingdom

[a] Author to whom correspondence should be addressed: pegg.james.t@gmail.com

ABSTRACT

The interaction of atomic and molecular hydrogen with actinide dioxide (AnO_2, An = U, Np, Pu) (111) surfaces has been investigated by DFT+U, where noncollinear 3k antiferromagnetic behaviour and spin-orbit interactions are considered. The adsorption of atomic hydrogen forms a hydroxide group, coupled to the reduction of an actinide ion. The energy of atomic hydrogen adsorption on the UO_2 (0.82 eV), NpO_2 (−0.10 eV), and PuO_2 (−1.25 eV) surfaces has been calculated. The dissociation of molecular hydrogen is not observed, shown to be due to kinetic rather than thermodynamic factors. As a barrier to the formation of a second hydroxyl group, an unusual charge distribution has been shown. This could be a limitation of a (1·1) unit cell method or an artefact of the systems. The recombination of hydrogen ions on the AnO_2 (111) surfaces is favoured over hydroxide formation.

https://doi.org/10.1063/1.5087577

I. INTRODUCTION

The corrosion of actinide materials concerns nuclear industries, where the radiolysis of organic compounds and other sources generate hydrogen.[1-6] This is known to catalyse the corrosion of the actinide metals.[7,8] Incidents involving corrosion have resulted in thermal excursions, expansion of solids, formation of incondensable gases, and containment failure.[9] The interaction of hydrogen with nuclear materials must be understood (imperative to the design of long-term storage facilities),[10] where the corrosion and oxidation of the actinide metals are often treated as equivalent topics.[11]

The actinide metals are highly reactive elements. The corrosion chemistry is controlled by the initial actinide dioxide (AnO_2) layer, formed by the unavoidable oxidation of the metal surface.[7,9,11-17] As an active template for the equilibration of the hydrogen-oxygen system, knowledge of the electronic structure of the AnO_2 is critical to the understanding of corrosion mechanisms.[5,18-20] A number of investigations have shown the AnO_2 (111) surface to be the most stable. The interpretation of the corrosion mechanism is highly complex, inferred from studies with hydrogen, oxygen, and water.[5,9] These involve the complex interplay of thermodynamic, kinetic, and catalytic factors.[11] A diffusion-controlled mechanism for oxygen migration across the oxide layer to the metal-oxide interface fails to account for hydrogen-catalysed oxidation and pyrophoric behaviour.[8,11,13,21,22] The influence of hydrogen on AnO_2 corrosion chemistry is unclear. Mechanisms for water-catalysed corrosion often incorporate the diffusion of hydrogen (H or H^+) or hydrogen-containing species (H_2O or OH) across the oxide surface layer to the metal-oxide interface.[23] In addition, the mechanism is thought to include the formation of hyperoxides (AnO_{2+x}) which increases the oxygen concentration gradient, thereby facilitating the migration of O^{2-} ions to the metal-oxide interface.

The interaction of hydrogen within the crystal structure and water adsorption has been investigated in earlier studies.[18-20,23-29]

The interplay of binding and formation energies has been shown to impact the thermodynamic stability of oxy-hydroxyl defects, where hydrogen stabilises isolated Willis clusters and greatly impacts the stability of oxygen clusters to form irreversible traps.[27,30] The occupation of octahedral interstitial sites (early AnO_2) or the formation hydroxyl groups (late AnO_2) by hydrogen has been shown to be controlled by the actinide element.[24] The formation energies of light impurity atoms (H, He, Li, Be, B, C, N, O, F, and Ne) are influenced by AnO_2.[24] The relative stability of the hydride ion compared to the hydroxyl group in UO_2 has been shown, where the uranium 5f electrons can form chemical bonds. The hydroxyl group is relatively stable in PuO_2 by contrast, where the plutonium 5f electrons are more localised.[23] The formation of hydroxyl groups on isostructural cerium dioxide (CeO_2) has also been found; however, cerium is a lanthanide element characterised by more simplistic behaviour.[31]

The interaction of hydrogen with AnO_2 surfaces is experimentally difficult to study.[12] The rate of corrosion is influenced by the extent of radiation damage, environmental conditions, and surface energetics. A limited number of experimental AnO_2 surface investigations have been published.[5,7–9,11–14,21,22,32] To compliment experimental investigations of AnO_2 surfaces, computational methods offer another method of study.[23–29] Although theoretical investigations are nontrivial,[15,16,33–35] the actinides are highly correlated f-electron systems for which conventional methods often fail. To calculate highly correlated systems, a number of methods have been developed. These include the self-interaction correction (SIC) method,[36] modified density functional theory (DFT+U),[37–41] hybrid density functionals,[42–44] and dynamic mean field theory (DMFT).[45] Of these methods, DFT+U is widely employed and offers a tractable means of study.

A fluorite-type structural motif is adopted by the AnO_2 under normal environmental conditions. At low temperature, the AnO_2 (An = U, Np, and Pu) show noncollinear 3k antiferromagnetic (AFM) behaviour.[46–51] The transverse 3k AFM state of UO_2 and NpO_2 results in $Pa\bar{3}$ (No. 205) crystal symmetry,[35] whereas the longitudinal 3k AFM state of PuO_2 results in $Fm\bar{3}m$ (No. 225) crystal symmetry.[34,52] In each instance, the external cubic symmetry is retained. In contrast with collinear 1k AFM states, a reduction of cubic crystal symmetry has been found.[34] The importance of spin-orbit interactions (SOI) in the actinide elements has been highlighted;[53] however, the impact of relativistic contributions is often ignored for computational simplicity.[54–56] Noncollinear magnetic behaviour is also infrequently considered.[34,52] The corrosion chemistry of the AnO_2 (111) surface is controlled by the electronic structure.[27] To mirror the corrosion chemistry of AnO_2, the electronic structure must be correctly calculated.[33]

The importance of noncollinear magnetic behaviour and spin-orbit interactions (SOI) on the electronic structure has been highlighted by a number of investigations.[6,33–35,52,53,55] In this paper, the interaction of hydrogen with the AnO_2 (An = U, Np, and Pu) (111) surface has been investigated by DFT+U. These calculations incorporate noncollinear 3k AFM behaviour and SOI influences. As the surface offers a nonuniform interface, inequivalent adsorption sites have been investigated. The electronic structure is compared against the clean surface, and this can be found in the supplementary material.[33]

II. COMPUTATIONAL METHODOLOGY

A. Calculation details

A noncollinear relativisitic study has been completed with the Vienna *Ab initio* Simulation Package (VASP) code.[36,45,57] A planewave basis set, relativistic effective core potentials (ECPs), and the frozen-core projector-augmented wave (PAW) method have been used.[43,58] The cut-off energy of the planewave basis set is 500 eV. The hydrogen ($1s^1$), oxygen ($2s^2$, $2p^4$), uranium ($6s^2$, $7s^2$, $6p^6$, $6d^2$ $5f^2$), neptunium ($6s^2$, $7s^2$, $6p^6$, $6d^2$ $5f^3$), and plutonium ($6s^2$, $7s^2$, $6p^6$, $6d^2$ $5f^4$) valence electrons are implicitly considered. The integration over the Brillouin zone with the Gaussian method has been completed.[59] Noncollinear magnetic wave-vectors and SOI are considered. The on-site Coulomb repulsion of the An 5f electrons is treated by the Liechtenstein *et al.* formulism, in which the Coulomb (U) and exchange (J) modifiers are treated as independent variables.[37–41] The exchange-correlation energy is evaluated by the revised Perdew-Burke-Ernzerhof for solid (PBEsol) functional, the improved performance of which
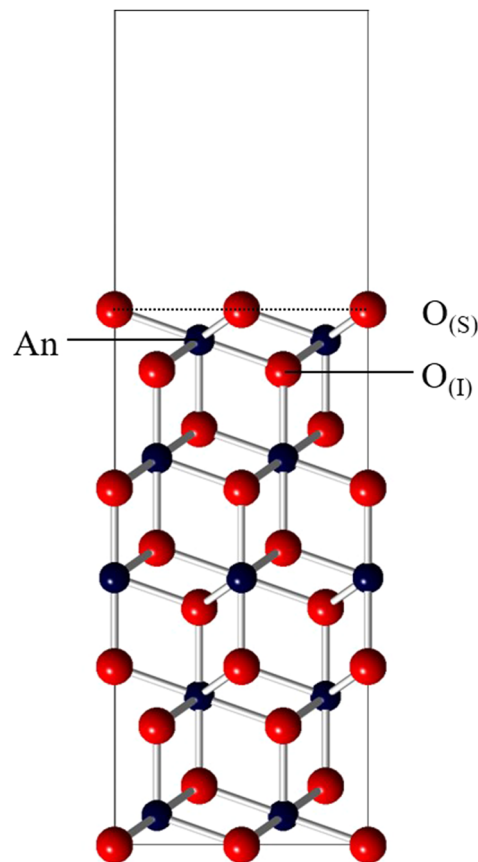

FIG. 1. The low-index AnO_2 (111) surface. The An^{4+} (blue) and O^{2-} (red) ions are indicated. The superior (primary layer, S) and inferior (tertiary layer, I) oxygen ions are labeled. The surface plane bisects the Os^{2-} ions as illustrated by the dashed black line. The surface model is comprised of 15 (5 O–An–O units) monolayers.

has been tested against other functionals.[52,60] In this study, all ions are fully relaxed with the conjugant gradient algorithm as implemented by VASP. The iteration threshold for electronic and ionic convergence is 1×10^{-5} eV and 1×10^{-2} eV·Å^{-1}, respectively.

A transverse 3k AFM state for UO_2 (U = 3.35 eV, J = 0.00 eV) and NpO_2 (U = 4.25 eV, J = 0.00 eV) with Pa$\bar{3}$ (No. 205, 0.014-0.016 Å distortion) crystal symmetry is used,[35] whereas for PuO_2, a longitudinal 3k AFM (U = 6.00 eV, J = 0.00 eV) model with Fm$\bar{3}$m (No. 225) crystal symmetry is used,[34] the implementation of which has already been documented. The surface is constructed from the ionically relaxed bulk structure with the METADISE code (Fig. 1).[16,61] The surface is formed of 15 monolayers (5 O–An–O units) with a vacuum gap of 20 Å; this is sufficient to isolate the surface from its periodic image. The convergence of the Γ-centred k-point grid (5·5·1) (recommended for hexagonal constructs) has been checked.[6,33,62]

B. Inequivalent positions

The adsorption of atomic H and molecular H_2 on the AnO_2 (111) surfaces is considered for multiple inequivalent lattice sites, where the influence of magnetic inequivalence is assumed to be negligible (Fig. 2). The inequivalent oxygen sites are differentiated by their position relative to the plane of the surface: superior (S) or inferior (I). The plane of the surface is defined as that which extends across the O_S^{2-} ions.

For molecular H_2, the orientation of the molecule is considered. In this study, molecular H_2 is either placed orthogonal (v) to the plane of the surface or parallel (n) along the direction of a bond. In each configuration, hydrogen is situated at a minimum of 1 Å above the plane of the surface. The implementation of a dipolar correction is not needed in our treatment; hydrogen is adsorbed on both sides of the model with inverse crystal symmetry. The seven inequivalent sites of the AnO_2 (111) surface include; three atomic [An, $O_{(S)}$, $O_{(I)}$] positions, three [An–$O_{(S)}$, An–$O_{(I)}$, $O_{(S)}$–$O_{(I)}$] bridging sites, and one interstitial (I) site. The ionic coordinates, magnetic vectors, and dimensions of the unit cell can be found in the supplementary material.[6,33]

C. Hydrogen adsorption

The hydrogen adsorption energy (E_{ads}) is calculated from the fully ionically relaxed cells. The total energy of the slab with the adsorbate ($E_{slab+absorbate}$), the energy of the adsorbate ($E_{absorbate}$), and the clean (adsorbate-free) slab energy (E_{slab}) are indicated

$$E_{ads} = 0.5(E_{slab+absorbate} - (E_{slab} + E_{absorbate})). \qquad (1)$$

The energy of the adsorbate ($E_{absorbate}$) is derived from the isolated H_2 molecule in a 10 Å^3 cubic cell. Integration of the Brillouin zone is completed with a 1·1·1 Γ-centred k-point mesh. The PBEsol calculations result in a H–H bond length (r_{H-H}) of 0.758 Å, in good agreement with the experimental value of 0.740 Å.[63] In terms of the adsorption energy, E_{ads}, negative values correspond to an energetically favourable exothermic process, while positive values correspond to an endothermic one. The adsorption energy (E_{ads}) is calculated from the full ionic relaxation. The dissociation energy of molecular H_2 (E_{ds} = 4.478 eV) has been measured by fluorescence-excitation spectroscopy.[64,65] A difference of 0.152 eV is introduced by PBEsol (E_{ds} = 4.630 eV), which can impact the calculation of adsorption energetics. To measure physisorption energies for H (~0.010-0.200 eV), the PBEsol error is considerable; however, to measure chemisorption energies for H (~1-2 eV), the PBEsol error is relatively insignificant. All models consider SOI.
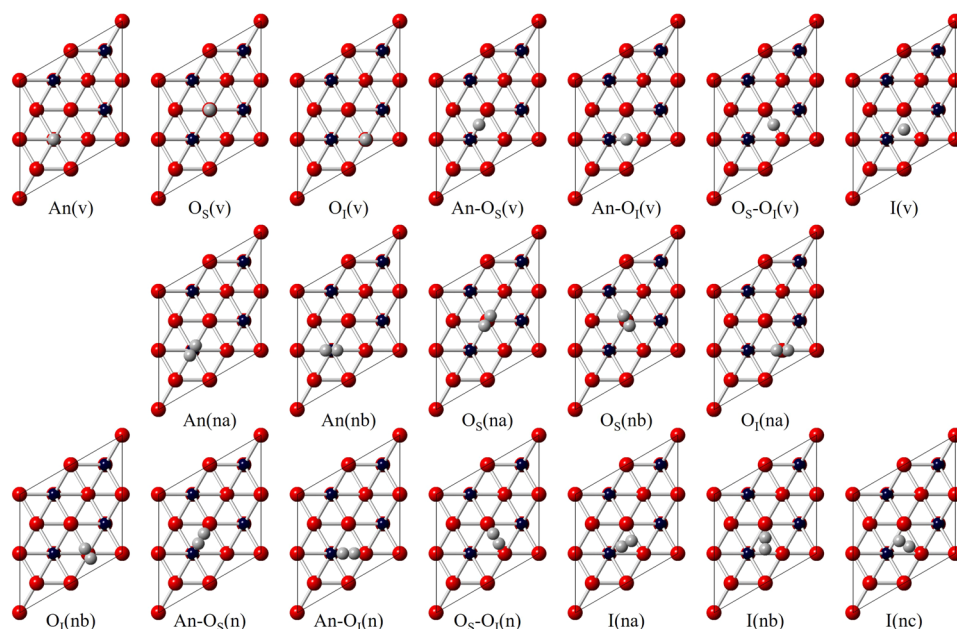

FIG. 2. The initial inequivalent configurations for the adsorption of atomic and molecular hydrogen on the AnO_2 (111) surface. The An^{4+} (blue) and O^{2-} (red) ions are indicated. The individual hydrogen positions are shown in grey. The minimum distance of the hydrogen atoms above the plane of the surface is 1 Å. The hydrogen molecule is considered with either orthogonal (v) or parallel (n) orientations relative to the surface plane.

III. RESULTS AND DISCUSSION

A. Uranium dioxide

Two interaction sites for atomic H–UO$_2$ (111) adsorption have been identified, both of which are endothermic in nature (Fig. 3). In hydrogenation and oxidation corrosion mechanisms, endothermic adsorption has been shown to be an important component.[66] The energetic ordering can be inferred from the position of the H s-band in the density of states (DoS), where lower energy states indicate a more stable configuration. In the high-energy aH$_{(111)}$ configuration, atomic H is located above an U ion and remains relatively isolated. The electronic structure is relatively unaffected, and no obvious hybrid OH sp-states are formed. The diagnosis is confirmed by the minimum U–H (2.001 Å) and O–H (2.589 Å) bond distance, which indicates that only weak interactions can occur. A weak hydride (H$^-$) ion from the Bader charge (−0.35 eV) has been indicated. In the low-energy bH$_{(111)}$ configuration, the interaction results in an unusual endothermic chemisorption mechanism. The formation of an OH ion is confirmed by the O–H bond distance (0.975 Å), hybrid OH sp-states (−9 eV to −8 eV), and Bader charge analysis (H = 0.61 eV). The corresponding reduction of an U ion is confirmed by the Bader charge reduction of the U (d) ion (2.55 eV to 2.19 eV) and the formation of the U f-defect in the bandgap. As the U (a-c) ions are closer in proximity to the H ion, the reduction of the outermost U (d) ion is unusual in terms of electrostatics.
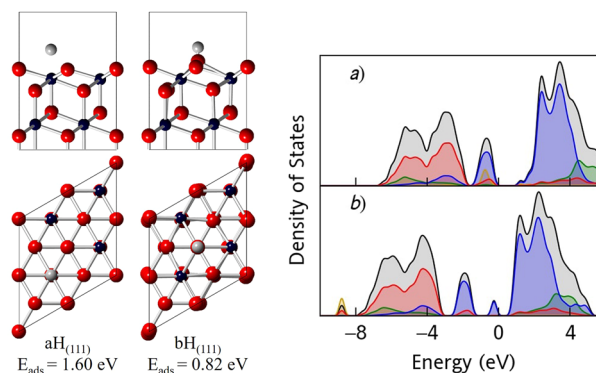

FIG. 3. The adsorption sites of atomic H on the UO$_2$ (111) surface. The U^{4+} (blue), O^{2-} (red), and H (grey) ions are indicated. The energy of adsorption (E$_{ads}$) is also shown. The density of states of the a-bH$_{(111)}$ configurations for the UO$_2$ (111) surface has been calculated. The total density of states (black), U f- (blue), U d- (green), O p- (red), and H s- (yellow) bands are coloured. Note: the hydrogen s-band has been magnified by a factor of 40 for clarity.

In earlier investigations with stoichiometric UO$_2$ models, hydride (H$^-$) ions are formed within interstitial sites.[26] The formation of the OH group was 0.27 eV higher in energy. It was also found that the compensating cation was distinct from the octahedral cage. The result indicates that reduction of the outermost cation is an
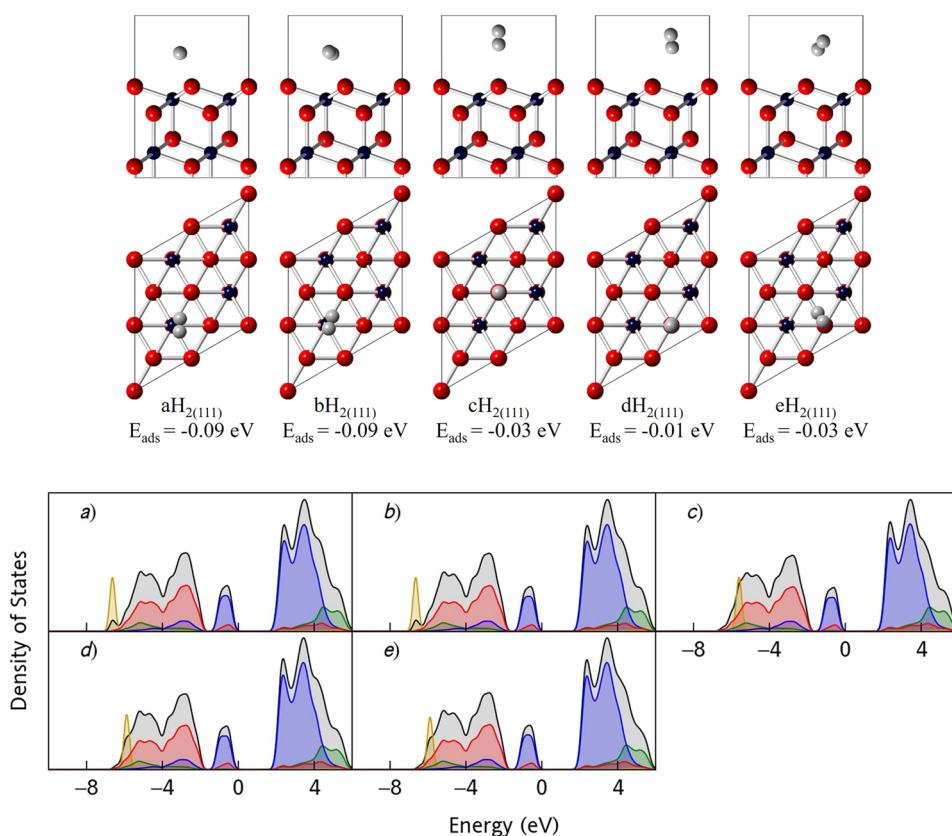

FIG. 4. The adsorption sites of molecular H$_2$ on the UO$_2$ (111) surface. The U^{4+} (blue), O^{2-} (red), and H (grey) ions are indicated. The energy of adsorption (E$_{ads}$) is also shown. The density of states of the a-eH$_{2(111)}$ configurations for the UO$_2$ (111) surface has been calculated. The total density of states (black), U f- (blue), U d- (green), O p- (red), and H s- (yellow) bands are coloured. Note that the hydrogen s-band has been magnified by a factor of 10 for clarity.

artefact of the system, where further experimental and computational investigation is needed. In contrast with hydrogen-surface interactions, the formation of an OH (0.975 Å) group is (0.78 eV) lower in energy; here, the surface offers an oxygen-rich region which can bind local high concentrations of hydrogen.[27]

The adsorption of molecular H_2 on the UO_2 (111) surface is non-dissociative, where five distinct [a-e$H_{2(111)}$] configurations have been found (Fig. 4). In each instance, molecular H_2 is adsorbed in the −0.01 eV to −0.10 eV energy range. In the low-energy a-b$H_{2(111)}$ configurations, molecular H_2 is located proximal to the U ion. In the a$H_{2(111)}$ configuration, the H ions occupy chemically equivalent positions and are slightly off-centre from the U ion, whereas in the b$H_{2(111)}$ configuration, the H ions are directed towards a nearby $O_{(S)}$ ion. The nearby electrostatic attraction to an $O_{(S)}$ ion is evident in each instance. If dissociation of the molecular H_2 were to occur, two mechanisms are possible: (1) the H ions separate uniformly along adjacent U–O(s) bonds forming chemically equivalent OH ions, (2) the H–H bond is elongated along a single U–O(s) bond forming an UH and OH pair. Although climbing nudged elastic band (cNEB) calculations are computationally unfeasible (due to the expense of noncollinear relativistic investigations), future investigations should consider these pathways.

In the c$H_{2(111)}$ configuration, molecular H_2 is located directly above an $O_{(S)}$ ion, offering another possibility for molecular H_2 dissociation, whereby one H ion initially forms an OH group. The dissociative mechanism could then proceed to the formation of a second OH group involving the remaining H ion. In the high-energy d$H_{2(111)}$ configuration, molecular H_2 is located above an $O_{(I)}$ ion orthogonal to the plane of the surface. Given the relatively high energetics of this configuration, it is unlikely to play any role in the dissociation of the H_2 molecule. In the e$H_{2(111)}$ configuration, molecular H_2 is proximal to the $O_{(I)}$ ion and directed towards the neighbouring $O_{(S)}$ ion, which is suggestive of the electrostatic attraction of hydrogen to the $O_{(S)}$ ion as a prelude to dissociation. The electronic structure for molecular H_2 adsorption on the UO_2 (111) surface, as indicated by the DoS, has been calculated for the a-e$H_{2(111)}$ configurations (Fig. 4). The absence of defect states or hybrid H s- and O p-states, in the a-e$H_{(111)}$ configurations, indicates that molecular H_2 is physisorbed. The magnitude of the electrostatic interaction is indicated by the position of the H s-band.

The dissociation of molecular H_2 is not observed on the UO_2 (111) surface, although there is clear evidence of atomic H chemisorption. The adsorption energies, DoS, and optimized geometries indicate that molecular H_2 is physisorbed onto the (111) surface, which is likely to be due to a large energetic barrier for the dissociation pathways relative to the energetically favourable (−0.10 eV to −0.01 eV) physisorption based on van der Waals interactions. A series of cNEB calculation could confirm this diagnosis. As of the unusual charge distribution in the atomic a$H_{(111)}$ configuration, the absence of dissociation may be a limitation of a (1·1) unit cell model. The charge distribution is unusual in terms of electrostatics, where the outermost surface An ion is reduced. In contrast, a (2·2) unit cell would offer the option of distributing the charge imparted by the adsorption of a H ion over a larger surface area. One notes that the distribution of charge and the separation of hydrogen ions over a greater surface would introduce a significant energetic barrier for dissociation.

As a limitation of noncollinear relativistic models, a full systematic study of a (2·2) unit cell is computationally unfeasible at this time.

B. Neptunium dioxide

An exothermic adsorption energy of −0.10 eV is calculated for the a$H_{(111)}$ configuration, formed by the interaction of atomic H on the NpO_2 (111) surface (Fig. 5). This differs from the endothermic adsorption energy of 0.82 eV for the UO_2 b$H_{(111)}$ configuration, although the configurations are structurally nearly identical. Atomic H is adsorbed directly above an $O_{(S)}$ ion, and the OH group is characterised by a bond length of 0.975 Å. In conjunction with the formation of an OH group, the Bader charge distribution confirms a H protonic state (Table A2). In contrast to atomic H adsorption on UO_2 (111) and PuO_2 (111) surfaces, no other stable configurations have been identified.

The formation of an OH group is confirmed by the hybridisation of the H s- and O p-states at −8 eV. The bandgap Np f-defect and the Bader charge analysis show the reduction of the Np (d) ion. The defect state reduces the bandgap of NpO_2 to 0.16 eV, and Mott-Hubbard characteristics are identified. In comparison with experimental data, the bandgap (0.40-3.10 eV) of NpO_2 differs considerably.[67–69] As hydrogen is notoriously difficult to remove from experimental studies, its impact on X-ray adsorption and epitaxial thin-film measurements is shown.[67–69]

The interaction of molecular H_2 on the NpO_2 (111) surface generates five distinct a-e$H_{2(111)}$ configurations (Fig. 6). The dissociation of molecular H_2 on the NpO_2 (111) surface (as with UO_2 and PuO_2) is not observed. The electronic structure indicates that molecular H_2 is physisorbed in each instance. In the low-energy a$H_{2(111)}$ configuration, molecular H_2 (E_{ads} = −0.10 eV) is located
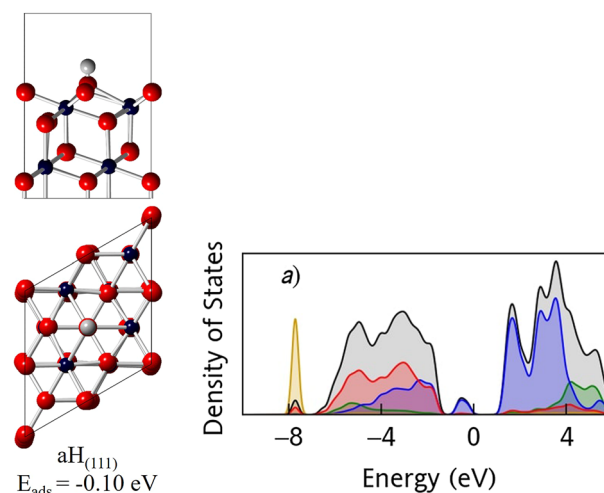

FIG. 5. The adsorption sites of atomic H on the NpO_2 (111) surface. The Np^{4+} (blue), $O^{2−}$ (red), and H (grey) ions are indicated. The energy of adsorption (E_{ads}) is also shown. The density of states of the a$H_{(111)}$ configuration for the NpO_2 (111) surface has been calculated. The total density of states (black), Np f- (blue), Np d- (green), O p- (red), and H s- (yellow) bands are coloured. Note that the hydrogen s-band has been magnified by a factor of 40 for clarity.
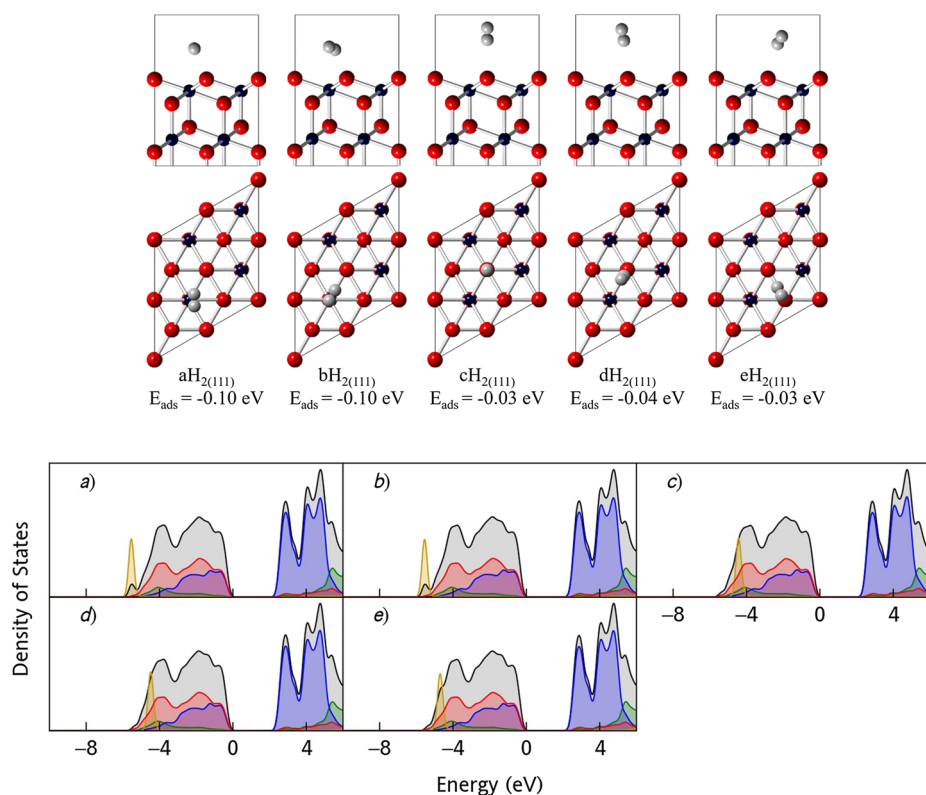
FIG. 6. The adsorption sites of molecular H_2 on the NpO_2 (111) surface. The Np^{4+} (blue), O^{2-} (red), and H (grey) ions are indicated. The energy of adsorption (E_{ads}) is also shown. The density of states of the a-e$H_{2(111)}$ configurations for the NpO_2 (111) surface has been calculated. The total density of states (black), Np f- (blue), Np d- (green), O p- (red), and H s- (yellow) bands are coloured. Note that the hydrogen s-band has been magnified by a factor of 10 for clarity.

above the Np ion. As the adoption energetics of atomic H and molecular H_2 are comparable, the dissociation of molecular H_2 is less favoured on the NpO_2 (111) surface.

By analysis of the Bader charge distribution of the atomic a$H_{(111)}$ state, a limitation of the (1·1) unit cell model employed is the inability to partition the electron density over a larger surface area. In addition, a large energetic barrier, introduced from the need to spread the negative charge over a greater distance, possibly hinders the formation of two OH groups. As such, even if molecular H_2 dissociates, recombination is highly probable. Given the surface areas involved in the distribution of charges, kinetic factors likely control the dissociation of molecular H_2 on the NpO_2 (111) surface. The dissociation mechanism may proceed by elongation of the H–H bond as each H ion moves towards an $O_{(S)}$ ion, or by the formation of a NpH and OH pair, with these mechanisms being analogues with those proposed for UO_2.

C. Plutonium dioxide

The interaction of hydrogen with the PuO_2 (111) surface results in a-b$H_{(111)}$ configurations (Fig. 7). The a$H_{(111)}$ configuration is characterised by an endothermic adsorption energy of 2.18 eV, whereas the b$H_{(111)}$ configuration is characterised by an exothermic adsorption energy of −1.25 eV. In the a$H_{(111)}$ configuration, the atomic H is positioned directly above a Pu ion. After a full ionic relaxation of hydrogen and the surface ions, the minimum Pu–H (2.403 Å) and O–H (2.754 Å) distances have been calculated. The configuration shares structural similarities with the UO_2

a$H_{(111)}$ configuration, although the endothermic energy of adsorption is considerably greater. In reference to the UO_2 b$H_{(111)}$ site and the NpO_2 a$H_{(111)}$ configurations, the PuO_2 b$H_{(111)}$ configuration is almost identical in terms of structural configuration. The energy of absorption decreases from 0.82 eV to −1.25 eV along the AnO_2
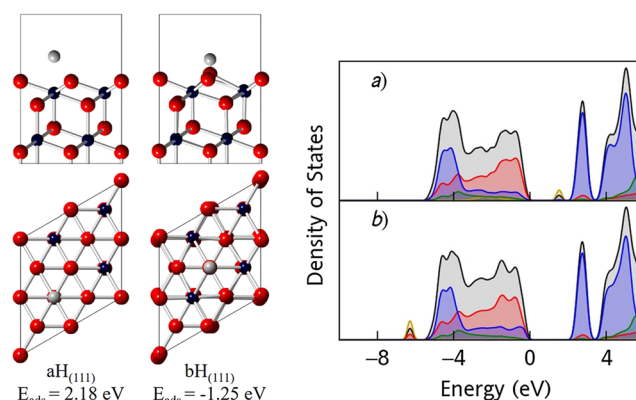

FIG. 7. The adsorption sites of atomic H on the PuO_2 (111) surface. The Pu^{4+} (blue), O^{2-} (red), and H (grey) ions are indicated. The energy of adsorption (E_{ads}) is also shown. The density of states of the a-b$H_{(111)}$ configurations for the PuO_2 (111) surface has been calculated. The total density of states (black), Pu f- (blue), Pu d- (green), O p- (red), and H s- (yellow) bands are coloured. Note that the hydrogen s-band has been magnified by a factor of 40 for clarity.

(An = U, Np, and Pu) series, which offers an indication of the increasing reactivity of the AnO_2 (111) surfaces. In the $bH_{(111)}$ site, the H atom is bonded to an $O_{(S)}$ atom to form an OH group, where the O–H bond distance of 0.976 Å is consistent with that of an OH group. The adsorption energy of −1.25 eV indicates an exothermic chemisorption mechanism. At the $O_{(S)}$ site, the neighbouring oxygen ions are drawn inwards, which results in a slight structural deformation. The formation of the OH group is confirmed by the H ion Bader charge of 0.58 eV (Table A3). This indicates a protonic state. In addition, the Pu (d) ion is reduced, whereas the O ions are only partially oxidised. In each instance, the electronic structure of the PuO_2 (111) surface is relatively unaffected and indicates molecular H_2 physisorption. As there is clear evidence of atomic H chemisorption on the PuO_2 (111) surface, it is perhaps surprising that the dissociation of molecular H_2 is not observed. As the charge cannot be distributed over a larger surface area, the $aH_{(111)}$ result implies a limitation of a (1·1) unit cell model. A large energetic barrier is thought to inhibit a dissociative adsorption mechanism, although cNEB calculations would markedly confirm the idea.

The instability of the $aH_{(111)}$ configuration is highlighted by the H s-defect state located within the bandgap. In the $bH_{(111)}$

configuration, the number of Pu f-states in the valence band has increased, whereas the number of Pu f-states in the conduction band has decreased. These changes indicate that high-energy Pu f-states (due to the interaction of hydrogen) are shifted to lower energy levels. The reduction of the formal Pu^{4+} (2.47 eV) ion to Pu^{3+} (2.08 eV) ion by hydrogen is confirmed by the Bader charge. Additionally, the hybridisation of the H s- and O p-states at 6 eV is indicative of the formation of an OH group.

In comparison, the interaction of molecular H_2 on the PuO_2 (111) surface results in four distinct $a\text{-}dH_{2(111)}$ configurations (Fig. 8). As with the UO_2 (111) and NpO_2 (111) surfaces, the dissociation of the molecular H_2 on the PuO_2 (111) surface is not observed. In each instance, the physisorption of molecular H_2 is in an energy range of −0.01 eV to −0.09 eV. The $aH_{2(111)}$ site, relative to the $bH_{2(111)}$ site, is marginally higher in energy by 0.01 eV. In both instances, molecular H_2 is positioned proximal to a Pu ion. In the $cH_{2(111)}$ site, molecular H_2 is located above an $O_{(S)}$ ion with an adsorption energy of −0.03 eV. The configuration potentially acts as an intermediate position for the dissociation of H_2 and the formation of an OH group. This is seen in the atomic $aH_{(111)}$ site; however, as stated, this has not been observed in these calculations. In addition, the $dH_{2(111)}$ site is reminiscent of the $cH_{2(111)}$
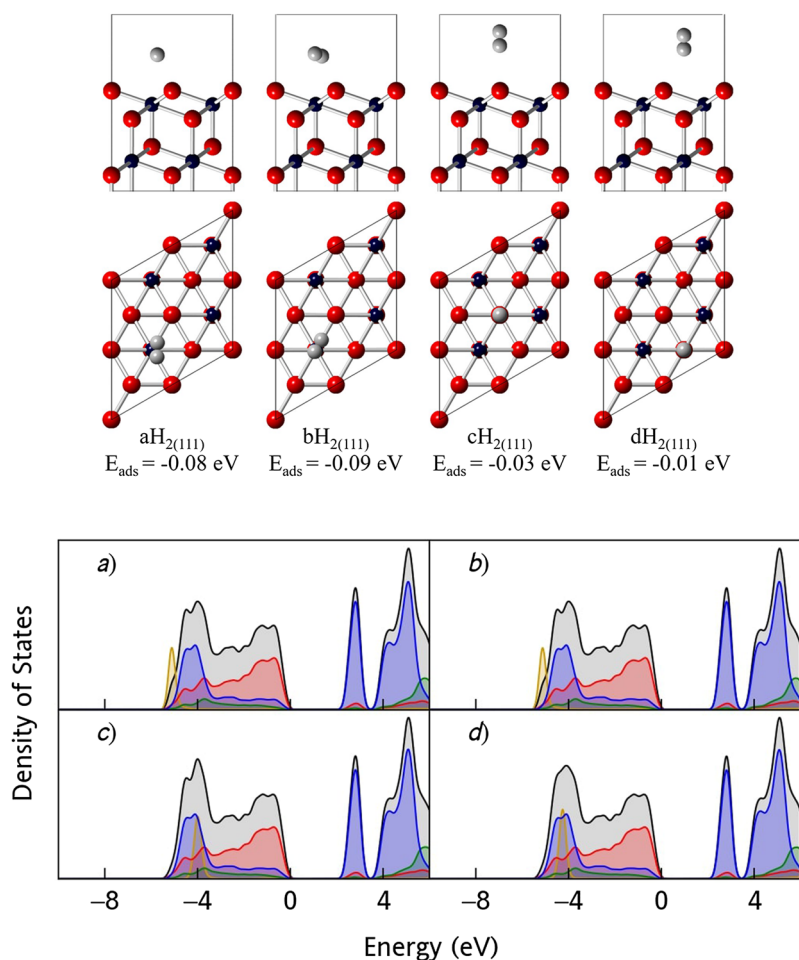

$aH_{2(111)}$
E_{ads} = -0.08 eV

$bH_{2(111)}$
E_{ads} = -0.09 eV

$cH_{2(111)}$
E_{ads} = -0.03 eV

$dH_{2(111)}$
E_{ads} = -0.01 eV

FIG. 8. The adsorption sites of molecular H_2 on the PuO_2 (111) surface. The Pu^{4+} (blue), $O^{2−}$ (red), and H (grey) ions are indicated. The energy of adsorption (E_{ads}) is also shown. The density of states of the $a\text{-}dH_{2(111)}$ configurations for the PuO_2 (111) surface has been calculated. The total density of states (black), Pu f- (blue), Pu d- (green), O p- (red), and H s- (yellow) bands are coloured. Note that the hydrogen s-band has been magnified by a factor of 10 for clarity.

site, although molecular H_2 is now located above the $O_{(I)}$ ion. The lowest-energy $bH_{2(111)}$ site is characterised by an adsorption energy of −0.09 eV. A physisorption mechanism is confirmed by the Bader charge distribution (Table A3). The disruption to the surface is negligible, and the hydrogen ions remain effectively charge neutral.

In each instance, the electronic structure of the PuO_2 (111) surface is relatively unaffected, which indicates molecular H_2 physisorption. As there is clear evidence of atomic H chemisorption on the PuO_2 (111) surface, it is perhaps surprising that the dissociation of molecular H_2 is not observed. A large energetic barrier is thought to influence the adsorption mechanism, which in future could be confirmed by cNEB calculations and the use of a (2·2) unit cell. This offers the option of distributing the charge imparted by the adsorption of a H ion over a larger surface area.

IV. CONCLUSIONS

The interactions of atomic H and molecular H_2 on the AnO_2 (An = U, Np, Pu) (111) surfaces has been investigated by DFT+U. The study considers SOI and noncollinear 3k AFM behaviour. The reactivity of the AnO_2 (111) surfaces increase along the U-Pu series. Multiple adsorption configurations were identified on the UO_2 and PuO_2 surfaces, while only one was found on NpO_2. In the interaction of atomic H with the AnO_2 (111) surfaces, an OH group is formed coupled with the reduction of an An ion. The energy of atomic H adsorption for UO_2 (0.82 eV), NpO_2 (−0.10 eV), and PuO_2 (−1.25 eV) is shown and is caused by increasing surface instability along the actinide series.[6] A clear shift from an endothermic to an exothermic mechanism is identified. The formation of the OH group is confirmed by the DoS and the Bader charge distribution. The structure of the low-energy UO_2 $bH_{(111)}$, NpO_2 $aH_{(111)}$, and PuO_2 $bH_{(111)}$ configurations is effectively identical.

The dissociation of molecular H_2 on the AnO_2 (111) surface is not observed; instead, molecular H_2 is weakly physisorbed. As the formation of the OH group is thermodynamically feasible, the dissociation of molecular H_2 is possibly hindered by kinetic factors. These observations can be explained in terms of the charge distribution, where the furthest actinide ion from the adsorption site is reduced. The inability to distribute charge is a key limitation of a (1·1) unit cell model, which is thought to hinder the formation of a second OH group. To incorporate the reduction of another An ion furthest away from the OH group, a second unit cell must be included within the model. Although a fully relativistic cNEB investigation is computationally intractable at this time, future investigations should consider the reaction pathways proposed in this study. The diffusion of hydrogen through the AnO_2 can be investigated by molecular dynamics. Investigation of hydrogen interactions with AnO_2 (011) and (001) surfaces for comparison are also planned.[6]

SUPPLEMENTARY MATERIAL

See supplementary material for the following information: Clean surface—fixed unit cell dimensions, ionic positions, magnetic structure, k-point convergence, and electronic density of states, and hydrogen interactions—ionic positions, magnetic structure, and Bader charges.

REFERENCES

[1] J. J. Katz, *The Chemistry of the Actinide and Transactinide Elements* (Springer Science and Business Media, 2007), Vols. 1–5.

[2] V. V. Rondinella and T. Wiss, "The high burn-up structure in nuclear fuel," Mater Today **13**(12), 24–32 (2010).

[3] M. Stan, "Discovery and design of nuclear fuels," Mater Today **12**(11), 20–28 (2009).

[4] J. R. Gregory, M. Astill, and M. G. Waine, "Reprocessing nuclear fuel," GB patent document 2031217/A/ (16 April 1980), available at http://inis.iaea.org/search/search.aspx?orig_q=RN:11564664.

[5] H. E. Sims, K. J. Webb, J. Brown, D. Morris, and R. J. Taylor, "Hydrogen yields from water on the surface of plutonium dioxide," J. Nucl. Mater. **437**(1), 359–364 (2013).

[6] J. T. Pegg, "A noncollinear relativistic computational study of the actinide dioxides and their interaction with hydrogen," Engineering Doctorate, University College London, UCL, 2018.

[7] J. M. Haschke, T. H. Allen, and J. C. Martz, "Oxidation kinetics of plutonium in air: Consequences for environmental dispersal," J. Alloys Compd. **271-273**, 211–215 (1998).

[8] J. M. Haschke, T. H. Allen, and J. L. Stakebake, "Reaction kinetics of plutonium with oxygen, water and humid air: Moisture enhancement of the corrosion rate," J. Alloys Compd. **243**(1-2), 23–35 (1996).

[9] J. M. Haschke, T. H. Allen, and L. A. Morales, "Reactions of plutonium dioxide with water and hydrogen–oxygen mixtures: Mechanisms for corrosion of uranium and plutonium," J. Alloys Compd. **314**(1-2), 78–91 (2001).

[10] R. C. Ewing, "Long-term storage of spent nuclear fuel," Nat. Mater. **14**(3), 252–257 (2015).

[11] J. M. Haschke, T. H. Allen, and L. A. Morales, "Surface and corrosion chemistry of plutonium," Los Alamos Sci. **26**(2), 252–273 (2000).

[12] L. Venault, A. Deroche, J. Gaillard, O. Lemaire, N. Budanova, J. Vermeulen *et al.*, "Dihydrogen H_2 steady state in α-radiolysis of water adsorbed on PuO_2 surface," Radiat. Phys. Chem. (published online).

[13] J. M. Haschke, "Corrosion of uranium in air and water vapor: Consequences for environmental dispersal," J. Alloys Compd. **278**(1-2), 149–160 (1998).

[14] J. M. Haschke, T. H. Allen, and L. A. Morales, "Reaction of plutonium dioxide with water: Formation and properties of PuO_{2+x}," Science **287**(5451), 285–287 (2000).

[15] A. E. Shields, *A Computational Analysis of Thorium Dioxide and $Th_{(1-x)} U_xO_2$ Systems* (University College London, UCL, 2015).

[16] A. E. Shields, D. Santos-Carballal, and N. H. de Leeuw, "A density functional theory study of uranium-doped thoria and uranium adatoms on the major surfaces of thorium dioxide," J. Nucl. Mater. **473**, 99–111 (2016).

[17] A. E. Shields, A. J. Miskowiec, J. L. Niedziela, M. C. Kirkegaard, K. Maheshwari, M. W. Ambrogio *et al.*, "Shining a light on amorphous U_2O_7: A computational approach to understanding amorphous uranium materials," Opt. Mater. **89**, 295–298 (2019).

[18]T. Bo, J.-H. Lan, C.-Z. Wang, Y.-L. Zhao, C.-H. He, Y.-J. Zhang *et al.*, "First-principles study of water reaction and H_2 formation on UO_2 (111) and (110) single crystal surfaces," J. Phys. Chem. C **118**(38), 21935–21944 (2014).

[19]T. Bo, J.-H. Lan, Y.-L. Zhao, Y.-J. Zhang, C.-H. He, Z.-F. Chai *et al.*, "Surface properties of NpO_2 and water reacting with stoichiometric and reduced NpO_2 (111), (110), and (100) surfaces from *ab initio* atomistic thermodynamics," Surf. Sci. **644**, 153–164 (2016).

[20]T. Bo, J.-H. Lan, Y.-L. Zhao, Y.-J. Zhang, C.-H. He, Z.-F. Chai *et al.*, "First-principles study of water adsorption and dissociation on the UO_2 (111), (110) and (100) surfaces," J. Nucl. Mater. **454**(1), 446–454 (2014).

[21]J. M. Haschke and T. H. Allen, "Plutonium hydride, sesquioxide and monoxide monohydride: Pyrophoricity and catalysis of plutonium corrosion," J. Alloys Compd. **320**(1), 58–71 (2001).

[22]J. M. Haschke and J. C. Martz, "Catalyzed corrosion of plutonium: Hazards and applications," Los Alamos Sci. **26**, 266–267 (2000).

[23]B. Ao, R. Qiu, H. Lu, and P. Chen, "Differences in the existence states of hydrogen in UO_2 and PuO_2 from DFT+U calculations," J. Phys. Chem. C **120**(33), 18445–18451 (2016).

[24]B. Ao, R. Qiu, G. Zhang, Z. Pu, X. Wang, and P. Shi, "Light impurity atoms as the probes for the electronic structures of actinide dioxides," Comput. Mater. Sci. **142**, 25–31 (2018).

[25]B. E. Tegner, M. Molinari, A. Kerridge, S. C. Parker, and N. Kaltsoyannis, "Water adsorption on AnO_2 {111}, {110}, and {100} surfaces (An = U and Pu): A density functional theory+U study," J. Phys. Chem. C **121**(3), 1675–1682 (2017).

[26]J. M. Flitcroft, M. Molinari, N. A. Brincat, M. T. Storr, and S. C. Parker, "Hydride ion formation in stoichiometric UO_2," Chem. Commun. **51**(90), 16209–16212 (2015).

[27]M. Flitcroft Joseph, M. Molinari, N. A. Brincat, N. R. Williams, M. T. Storr, G. C. Allen *et al.*, "The critical role of hydrogen on the stability of oxy-hydroxyl defect clusters in uranium oxide," J. Mater Chem. A **6**(24), 11362–11369 (2018).

[28]J. Glascott, "A model for the initiation of reaction sites during the uranium–hydrogen reaction assuming enhanced hydrogen transport through linear oxide discontinuities," Philos. Mag. **94**(13), 1393–1413 (2014).

[29]J. Glascott, "A model for the initiation of reaction sites during the uranium–hydrogen reaction assuming enhanced hydrogen transport through thin areas of surface oxide," Philos. Mag. **94**(3), 221–241 (2014).

[30]N. A. Brincat, M. Molinari, S. C. Parker, G. C. Allen, and M. T. Storr, "Computer simulation of defect clusters in UO_2 and their dependence on composition," J. Nucl. Mater. **456**, 329–333 (2015).

[31]M. Fronzi, S. Piccinin, B. Delley, E. Traversa, and C. Stampfl, "Water adsorption on the stoichiometric and reduced CeO_2(111) surface: A first-principles investigation," Phys. Chem. Chem. Phys. **11**(40), 9188–9199 (2009).

[32]J. M. Haschke, H. K. Fauske, and A. G. Phillips, "Pyrophoric potential of plutonium-containing salt residues," J. Nucl. Mater. **279**(2-3), 127–138 (2000).

[33]J. T. Pegg, A. E. Shields, M. T. Storr, D. O. Scanlon, and N. H. de Leeuw, "Noncollinear relativistic DFT+U calculations of actinide dioxide surfaces," J. Phys. Chem. C **123**(1), 356–366 (2019).

[34]J. T. Pegg, A. E. Shields, M. T. Storr, A. S. Wills, D. O. Scanlon, and N. H. de Leeuw, "Hidden magnetic order in plutonium dioxide nuclear fuel," Phys. Chem. Chem. Phys. **20**(32), 20943–20951 (2018).

[35]J. T. Pegg, A. E. Shields, M. T. Storr, A. S. Wills, D. O. Scanlon, and N. H. de Leeuw, "Magnetic structure of UO_2 and NpO_2 by first-principle methods," Phys. Chem. Chem. Phys. **21**(2), 760–771 (2019).

[36]J. P. Perdew and A. Zunger, "Self-interaction correction to density-functional approximations for many-electron systems," Phys. Rev. B **23**(10), 5048–5079 (1981).

[37]P. Hohenberg and W. Kohn, "Inhomogeneous electron gas," Phys. Rev. **136**(3B), B864–B71 (1964).

[38]W. Kohn and L. J. Sham, "Self-consistent equations including exchange and correlation effects," Phys. Rev. **140**(4A), A1133–A1138 (1965).

[39]S. L. Dudarev, G. A. Botton, S. Y. Savrasov, C. J. Humphreys, and A. P. Sutton, "Electron-energy-loss spectra and the structural stability of nickel oxide: An LSDA+U study," Phys. Rev. B **57**(3), 1505–1509 (1998).

[40]A. I. Liechtenstein, V. I. Anisimov, and J. Zaanen, "Density-functional theory and strong interactions: Orbital ordering in Mott-Hubbard insulators," Phys. Rev. B **52**(8), R5467–R5470 (1995).

[41]V. I. Anisimov, J. Zaanen, and O. K. Andersen, "Band theory and Mott insulators: Hubbard U instead of stoner I," Phys. Rev. B **44**(3), 943–954 (1991).

[42]C. Adamo and V. Barone, "Toward reliable density functional methods without adjustable parameters: The PBE0 model," J. Chem. Phys. **110**(13), 6158–6170 (1999).

[43]J. Heyd, G. E. Scuseria, and M. Ernzerhof, "Hybrid functionals based on a screened Coulomb potential," J. Chem. Phys. **118**(18), 8207–8215 (2003).

[44]I. D. Prodan, G. E. Scuseria, and R. L. Martin, "Covalency in the actinide dioxides: Systematic study of the electronic properties using screened hybrid density functional theory," Phys. Rev. B **76**(3), 033101 (2007).

[45]A. Georges, G. Kotliar, W. Krauth, and M. J. Rozenberg, "Dynamical mean-field theory of strongly correlated fermion systems and the limit of infinite dimensions," Rev. Mod. Phys. **68**(1), 13 (1996).

[46]P. W. Anderson, "Antiferromagnetism. Theory of superexchange interaction," Phys. Rev. **79**(2), 350–356 (1950).

[47]R. Caciuffo, N. Magnani, P. Santini, S. Carretta, G. Amoretti, E. Blackburn *et al.*, "Anisotropic magnetic fluctuations in 3-k antiferromagnets," J. Magn. Magn. Mater. **310**(2, Part 2), 1698–1702 (2007).

[48]P. Giannozzi and P. Erdös, "Theoretical analysis of the 3-k magnetic structure and distortion of uranium dioxide," J. Magn. Magn. Mater. **67**(1), 75–87 (1987).

[49]W. Kopmann, F. J. Litterst, H. H. Klauß, M. Hillberg, W. Wagener, G. M. Kalvius *et al.*, "Magnetic order in NpO_2 and UO_2 studied by muon spin rotation," J. Alloys Compd. **271-273**, 463–466 (1998).

[50]D. Mannix, G. H. Lander, J. Rebizant, R. Caciuffo, N. Bernhoeft, E. Lidström *et al.*, "Unusual magnetism of NpO_2: A study with resonant X-ray scattering," Phys. Rev. B **60**(22), 15187–15193 (1999).

[51]P. Santini, R. Lémanski, and P. Erdős, "Magnetism of actinide compounds," Adv. Phys. **48**(5), 537–653 (1999).

[52]J. T. Pegg, X. Aparicio-Anglès, M. Storr, and N. H. de Leeuw, "DFT+U study of the structures and properties of the actinide dioxides," J. Nucl. Mater. **492**, 269–278 (2017).

[53]G. van der Laan, K. T. Moore, J. G. Tobin, B. W. Chung, M. A. Wall, and A. J. Schwartz, "Applicability of the spin-orbit sum rule for the actinide 5f states," Phys. Rev. Lett. **93**(9), 097401 (2004).

[54]Z. Rák, R. C. Ewing, and U. Becker, "Hydroxylation-induced surface stability of AnO_2 (An = U, Np, Pu) from first-principles," Surf. Sci. **608**, 180–187 (2013).

[55]S. A. Moten, R. Atta-Fynn, A. K. Ray, and M. N. Huda, "Size effects on the electronic and magnetic properties of PuO_2 (111) surface," J. Nucl. Mater. **468**, 37–45 (2016).

[56]J. Boettger and A. Ray, "Fully relativistic density functional calculations on hydroxylated actinide oxide surfaces," Int. J. Quantum Chem. **90**(4-5), 1470–1477 (2002).

[57]V. I. Anisimov, *Strong Coulomb Correlations in Electronic Structure Calculations* (CRC Press, 2000).

[58]J. Heyd, G. E. Scuseria, and M. Ernzerhof, "Erratum: 'Hybrid functionals based on a screened Coulomb potential' [J. Chem. Phys. 118, 8207 (2003)]," J. Chem. Phys. **124**(21), 219906 (2006).

[59]P. E. Blöchl, O. Jepsen, and O. K. Andersen, "Improved tetrahedron method for Brillouin-zone integrations," Phys. Rev. B **49**(23), 16223 (1994).

[60]G. I. Csonka, J. P. Perdew, A. Ruzsinszky, P. H. Philipsen, S. Lebègue, J. Paier *et al.*, "Assessing the performance of recent density functionals for bulk solids," Phys. Rev. B **79**(15), 155107 (2009).

[61]G. W. Watson, E. T. Kelsey, N. H. de Leeuw, D. J. Harris, and S. C. Parker, "Atomistic simulation of dislocations, surfaces and interfaces in MgO," J. Chem. Soc., Faraday Trans. **92**(3), 433–438 (1996).

[62]W. Sun and G. Ceder, "Efficient creation and convergence of surface slabs," Surf. Sci. **617**, 53–59 (2013).

[63]R. C. Weast, M. J. Astle, and W. H. Beyer, *CRC Handbook of Chemistry and Physics* (CRC Press, Boca Raton, FL, 1988).

[64]A. Balakrishnan, V. Smith, and B. P. Stoicheff, "Dissociation energy of the hydrogen molecule," Phys. Rev. Lett. **68**(14), 2149–2152 (1992).

[65] G. Herzberg, "The dissociation energy of the hydrogen molecule," J. Mol. Spectrosc. **33**(1), 147–168 (1970).

[66] J. H. De Boer, "50 endothermic chemisorption and catalysis," in *Advances in Catalysis*, edited by A. Farkas (Academic Press, 1957), Vol. 9, pp. 472–480.

[67] T. M. McCleskey, E. Bauer, Q. Jia, A. K. Burrell, B. L. Scott, S. D. Conradson *et al.*, "Optical band gap of NpO_2 and PuO_2 from optical absorbance of epitaxial films," J. Appl. Phys. **113**(1), 013515 (2013).

[68] P. Erdös, G. Solt, Z. ⊙ołnierek, A. Blaise, and J. M. Fournier, "Magnetic susceptibility and the phase transition of NpO_2," Physica B+C. **102**(1), 164–170 (1980).

[69] C. Suzuki, T. Nishi, M. Nakada, M. Akabori, M. Hirata, and Y. Kaji, "Core-hole effect on XANES and electronic structure of minor actinide dioxides with fluorite structure," J. Phys. Chem. Solids **73**(2), 209–216 (2012).